JOURNAL OF PROPULSION AND POWER
Vol. 18, No. 1, January–February 2002

Flow Past Stationary Spherical Particles with Streamwise Velocity Fluctuation

A. Dasgupta*
Quest, Inc., Flint, Michigan 48507
and
T. I-P. Shih†
Michigan State University, East Lansing, Michigan 48824

Computations were performed to investigate flow past stationary spherical particles with and without an imposed sinusoidal fluctuation in the streamwise velocity upstream of the particles at two different particle Reynolds numbers (50 and 100). When there is an imposed velocity fluctuation, the amplitude of the velocity fluctuation was kept at 0.05 of the mean velocity magnitude, and five wavelengths (2*D*, 4*D*, 5*D*, 7*D*, 10*D*; *D* is particle diameter) were investigated. The focus of the computations is to understand how wavelength of velocity fluctuation affects drag, surface pressure, and surface shear for the following three particle problems: 1) an isolated single particle, 2) four particles-in-tandem along the fluctuating-flow direction, and 3) an array of particles arranged in a nonstaggered fashion. Results show the drag, friction, and pressure coefficients to be strong functions of the wavelength of velocity fluctuation. Also, the fluctuating velocity was found to change the point of flow separation. For the single particle problem, velocity fluctuations were found to increase the drag coefficient. For the problems involving particles in tandem and an array of particles, velocity fluctuations were found to decrease the drag coefficient due to particle interactions. This study is based on the conservation equations of mass, momentum (full compressible Navier–Stokes), and energy for three-dimensional, unsteady, laminar flows of an ideal gas with constant specific heats. Solutions were generated by using a second-order-accurate finite volume method based on Newton–Raphson iteration and a diagonalized alternating-direction implicit scheme on overlapped grids.

Nomenclature

A_c	=	particle cross-sectional area ($A_c = \pi D^2/4$)
C_D	=	drag coefficient ($C_D =$ total drag/$\frac{1}{2}\rho u_0^2 A_c$)
$\bar{C}_D$	=	drag coefficient averaged over one fluctuation period
$C_{D,f}$	=	friction drag coefficient ($C_{D,f} =$ friction drag/$\frac{1}{2}\rho u_0^2 A_c$)
$\bar{C}_{D,f}$	=	friction coefficient averaged over one fluctuation period
$C_{D,p}$	=	pressure drag coefficient ($C_{D,p} =$ pressure drag/$\frac{1}{2}\rho u_0^2 A_c$)
$\bar{C}_{D,p}$	=	pressure coefficient averaged over one fluctuation period
C_f	=	friction coefficient ($C_f =$ local shear/$\frac{1}{2}\rho u_0^2$)
C_p	=	pressure coefficient ($C_p =$ local pressure/$\frac{1}{2}\rho u_0^2$)
D	=	particle diameter
Re	=	particle Reynolds number ($Re = \rho u_0 D/\mu$)
t	=	time
U	=	vector of dependent variables ($U = [\rho, \rho u, \rho v, \rho w, e]^T$)
u, v, w	=	x, y, z component of the velocity
u_0	=	mean x component velocity at inflow boundary
u'	=	amplitude of velocity fluctuation about mean at inflow boundary [Eq. (1a)]
x, y, z	=	Cartesian coordinate system
α	=	particle volume fraction for the particle-array problem ($\alpha = (\pi D^3/6)/\ell^3$, $\ell =$ spacing between particles measured from particle center; Fig. 3)
λ	=	wavelength of velocity fluctuation at inflow boundary [Eq. (1b)]
μ	=	dynamic viscosity
ξ, η, ζ	=	boundary-fitted coordinates
ρ	=	density
τ	=	time in boundary-fitted coordinate system ($\tau = t$)
ω	=	frequency of velocity fluctuation at inflow boundary [Eq. (1b)]

Received 20 January 1996; revision received 11 September 2001; accepted for publication 11 September 2001.

*Project Engineer, Quest Automotive.
†Professor, Department of Mechanical Engineering. Associate Fellow AIAA.

Introduction

LIQUID sprays and particle-laden flows are utilized in many applications of practical importance. For these flows, it is important to understand the interactions between the particles (liquids or solids) and the fluid (gases or liquids) in which they are dispersed. Many investigators have studied particle/particle and particle/fluid interactions by using both experimental and mathematical methods. Experimental studies of such flows have provided lumped overall effects such as drag, but have not yet reported the detailed flow around each particle because of measurement difficulties (see, e.g., Refs. 1–4, and the references cited there). Mathematical studies that reveal detailed flow about each particle can be classified according to the range of the particle Reynolds number investigated (i.e., the Reynolds number based on particle diameter and particle-fluid relative velocity). When the particle Reynolds number is either extremely low (creeping flow) or extremely high (potential flow), certain asymptotic approximations can be invoked. For these extreme limits of the particle Reynolds number, considerable capabilities have been developed.[5–7] But, many flows of practical importance involve particle Reynolds numbers in the low to the intermediate range, where the asymptotic approximations cannot be invoked, and the full Navier–Stokes equations must be used.

A number of investigators have used the full Navier–Stokes equations to study the flow past or induced by multiple particles.[8–17]

When the full Navier–Stokes equations are used, it is not feasible at this time to perform rigorous analysis on complete sprays and particle-ladenflows because of their enormous complexities.[4,18] The approach, taken to understand the nature of the flow around individual particles, has been to study a few particles in well-defined arrangements (e.g., along a line parallel or perpendicular to the main flow) and in idealized environments (e.g., uniform flow or uniform shear). So far, no computational studies have been reported on fluctuating flow past multiple particles based on the full Navier–Stokes equations. Such a study can lead to better understanding of particle/particle and particle/fluid interactions under turbulent flow conditions. Here, it is noted that a study on oscillating flow about a single particle was reported by Duvvur et al.[19] In their study the focus was on vaporization of a fuel droplet.

The objective of this study is to investigate fluctuating flow past single and multiple solid particles that are stationary and spherical in shape. The focus is on understanding how wavelength of velocity fluctuations in the streamwise direction affect drag, shear, and pressure for three particle problems: 1) an isolated single particle, 2) four particles in tandem along the main flow direction, and 3) an array of particles arranged in a nonstaggered fashion.

The remainder of this paper is organized as follows. The three particle problems investigated are described in the next section. The subsequent sections give the problem formulation, the numerical method of solution, the validation process, and the results generated.

Description of Problem

All particle problems investigated involve air flowing past perfectly insulated, stationary, spherical particles of the same diameter D with the flow in the laminar regime. The first problem investigated is depicted in Fig. 1. It entails fluctuating flow past an isolated, single particle. Henceforth, this problem is referred to as the "single-particle problem."

The second problem investigated is depicted in Fig. 2. This problem entails fluctuating flow past four particles that are all located along one line parallel to the direction of the main flow. Henceforth, this problem is referred to as the "particles-in-tandem problem."

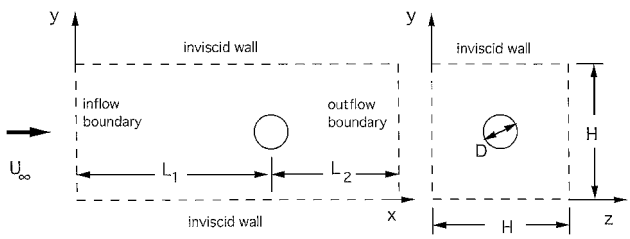

Fig. 1 Schematic diagram of single-particle problem.

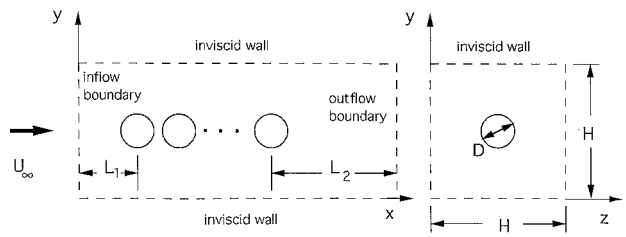

Fig. 2 Schematic diagram of particles-in-tandem problem.

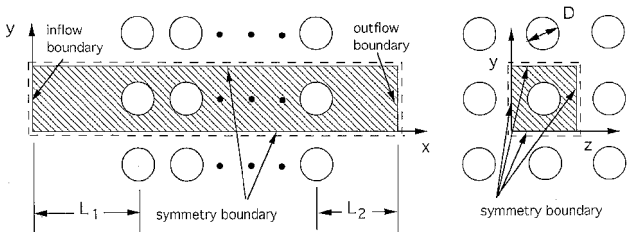

Fig. 3 Schematic diagram of particle-array problem.

For this problem the particles in tandem are always equally spaced with the separation distance, measured between the centers of the particles, being two dimensional.

The third problem investigated is depicted in Fig. 3. This problem entails fluctuating flow past an array of equally spaced particles that are arranged in a nonstaggered fashion in which each particle (except for those on the boundaries of the array) is surrounded by particles both along and in two directions perpendicular to the flow. Henceforth, this problem will be referred to as the "particle-array problem." For this problem several different spacings between the particles that give rise to different particle volume fractions were investigated as explained in the Results section.

The computational domain for each of the three problems just described and depicted in Figs. 1–3 is the region bounded by the dashed lines. The sizes of the domains for the first two problems, depicted in Figs. 1 and 2, were arrived at by numerical experiments to ensure that they are sufficiently large to mimic uniform flow past particles in an infinitely large domain as explained in the section on validation. For the third problem, depicted in Fig. 3, because of symmetry only one row of particles along the flow direction needs to be analyzed.

For all three problems the fluctuating flow was induced at the inflow boundary through the following boundary condition (BC) for the streamwise velocity:

$$u = u_0 + u' \cos(\omega\tau), \qquad v = w = 0 \tag{1a}$$

$$\omega = 2\pi u_0/\lambda \tag{1b}$$

In this study u'/u_0 was fixed at 0.05; u_0 was varied to give particle Reynolds numbers ($Re = \rho u_0 D/\mu$) of 50 and 100; ω was varied to give wavelengths of the velocity fluctuations (λ) of $2D$, $4D$, $5D$, $7D$, and $10D$. D is chosen so that the Keulegan–Carpenter number ($2\pi u'/D$) is always much less than unity.

The other BCs at the inflow boundary were constant static temperature and pressure, which imply the stagnation temperature and pressure oscillate at the inflow boundary. Because all variables were specified at the inflow boundary and the flow is subsonic throughout the domain, all variables at the outflow boundary were extrapolated (i.e., the second derivative of velocity, temperature, and pressure were set to zero). At both the inflow and the outflow boundaries density was computed by using the ideal gas equation of state. The BCs used at the inflow and outflow boundaries allow the velocity fluctuations to be controlled in an easy manner. With Eq. (1) the flow must be compressible in order to satisfy the continuity equation. Thus, the velocity fluctuations at the inflow boundary induce oscillations in pressure, temperature, and density throughout the flowfield.

Additional details on the geometry, flow conditions, as well as the range of parameters investigated, about the three problems depicted in Figs. 1–3, are given in the sections on problem formulation and results.

Problem Formulation

The equations governing the oscillating flow past stationary particles are taken to be the unsteady, three-dimensional form of the conservation equations of mass (continuity), momentum (full Navier–Stokes), and total energy for compressible, laminar flow of a thermally and calorically perfect gas with Sutherland's model for viscosity and constant Prandtl number. These equations can be written in generalized coordinates and cast in the following strong conservation-law form:

$$\frac{\partial JU}{\partial \tau} + \frac{\partial F}{\partial \xi} + \frac{\partial G}{\partial \eta} + \frac{\partial H}{\partial \zeta} = 0 \tag{2}$$

In the preceding equation, $J = |\partial(x, y, z, t)/\partial(\xi, \eta, \zeta, \tau)|$ is the determinant of the Jacobian of the transformation from the (x, y, z, t) coordinate system to the (ξ, η, ζ, τ) coordinate system; $U = [\rho, \rho u, \rho v, \rho w, e]^T$ is the vector of dependent variables (superscript T denotes transpose); e is thermal and mechanical energy

per unit volume; and F, G, and H are the flux vectors, representing inviscid and viscous transport of mass, momentum, and energy. Because the preceding representation of the conservation equations is well known,[20] further details are not given.

To obtain solutions to the conservation equations, boundary and initial conditions are needed. The BCs employed in this study for the different boundaries shown in Figs. 1–3 are as follows. The BCs imposed at the inflow and outflow boundaries are given in the preceding section. The BCs imposed on the inviscid walls are slip surface and adiabatic wall. The BCs imposed at the particle surfaces are the no-slip condition and adiabatic wall. The BCs imposed at symmetry boundaries are zero derivatives of the dependent variables except for the velocity component normal to those boundaries, which is set equal to zero. The initial conditions imposed are uniform flow at u_0 with constant density and pressure.

Numerical Method of Solution

Solutions to the conservation equations of mass, momentum, and total energy given by Eq. (2) were obtained by using a modified version of the OVERFLOW code.[15,21] The OVERFLOW code contains many algorithms. The one used in this study is as follows: All inviscid and viscous terms were centrally differenced. The central differencing of the inviscid terms was stabilized by adding fourth-order artificial dissipation. Because transient solutions are of interest, the time-derivative terms were approximated by the second-order accurate, three-point backward formula. The system of nonlinear equations that resulted from the aforementioned approximations to the space and time derivatives was analyzed by using Newton–Raphson iteration with a diagonalized alternating-direction scheme.[22]

For each of the three particle problems, an overlapping chimera grid system[23,24] was employed to represent the domain. Each chimera grid involves two types of grids—a main grid and a number of minor grids that overlap the main grid. The main grid covers the entire domain (region enclosed by the dashed lines) as if there are no particles in the domain. The minor grids are for the particles with one minor grid for each particle. Thus, for the single-particle problem depicted in Fig. 1, there are one main grid and one minor grid. For the particles-in-tandem and particle-array problem depicted in Figs. 2 an 3, there is one main grid and four minor grids.

A representative chimera grid system employed in this study is shown in Fig. 4a for the particle-array problem. The main grid has an H-H grid structure in which the grid spacing in the x, y, and z directions are all the same in the region that included the particles but became larger as the distance from the leading or trailing particle increased. The minor grid that surrounds each particle has an O-O structure with grid points clustered next to the particle surface. The O-O structure has a periodic boundary along which periodic boundary conditions were imposed. The O-O grid also has a line of singularity, which can cause numerical difficulties. This line of singularity can be eliminated by overlapping an H-H grid to cover it, but was found to be unnecessary in this study because the fine grid employed permitted an averaging boundary condition to be applied there.

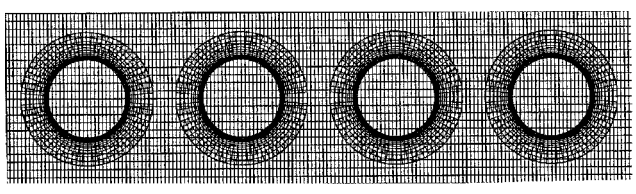

a) Overlapped major and minor grids

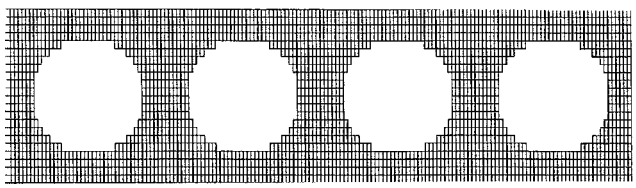

b) Major grid with holes punched in it

Fig. 4 Chimera grid system in the region about the particles.

After the main and the minor grids have been generated, holes are punched into the main grid, one for each minor grid, at locations where the particles are to be located (see Fig. 4b). Because the hole boundaries in the main grid and the outer boundaries of the minor grids are internal boundaries, where data should flow across freely, these boundaries are completely embedded in each other (i.e., the hole boundaries are embedded in the appropriate minor grids, and the boundary of the minor grids are all embedded in the main grid) so that data can be transferred between the grids by interpolation. Additional details, about the grid systems employed for the three problems studied including the number of grid points and their distribution, are given in the section on validation.

During computations, the flowfield in each grid was analyzed one at a time. Information from one grid was passed to another grid via trilinear interpolation at grid boundaries. The required interpolation coefficients were obtained by using the PEGSUS code.[23,24] This process of analyzing the flow in one grid at a time until all grids are analyzed was repeated for each time step until a converged unsteady solution has been obtained for that time step.

Validation

Before the modified OVERFLOW code, which embodies the formulation and the numerical method of solution described in the preceding two sections, can be used to study flow past particles, it must be validated. The validation of this code was made by performing computations of steady flow past an isolated single spherical particle. This problem was selected because experimental and numerical data exist in the literature (see, e.g., Refs. 25–28), which can be used for comparison.

The validation process is as follows. First, steps were taken to determine the minimum dimensions for L_1, L_2, and H (see Fig. 1) needed to mimic uniform flow past an isolated single particle. Next, the number and distribution of grid points needed to obtain grid-independent solutions were determined. Finally, computed results were compared with experimental and numerical data in the literature.

With regard to domain size, it was found that L_1, L_2, and H must be greater than or equal to $25D$, $10D$, and $\sqrt{(50\pi)}D$, respectively. In this study the minimum values were used for the three problems depicted in Figs. 1–3.

With regard to grid-independent solutions, it was found that the computed drag and point of separation on the particle varied by less than 1%, when grid spacings were halved if the minor grid around the particle and the major grid that covered the entire domain satisfied the following conditions. For the minor grid with an O-O structure, the minimum number of grid lines needed are $IL = 12$ in the radial direction, $JL = 37$ in the latitudinal direction (spanning π radians), and $KL = 73$ in the longitudinal direction (spanning 2π radians). For this O-O grid, grid lines were equally distributed in the latitudinal and longitudinal directions, but clustered in the radial direction next to the particle surface in a geometric progression according to

$$\Delta r_i = r_i - r_{i-1} = a P^{i-1}, \qquad i = 1, 2, \ldots, IL \tag{3}$$

where $a = 0.005D$ and P must be less than or equal to 1.24 with $i = 1$ corresponding to the particle surface (i.e., $r_1 = D/2$). For the major grid with an H-H structure, the grid spacing was small over a region close to the particle and became larger as the distance from the particle increased. In the region closest to the particle, grid lines were equally spaced in all directions with $\Delta x = \Delta y = \Delta z = b$, where b must be less than or equal to $(D/2 + \Delta r_2 + \Delta r_3 + \cdots + \Delta r_{IL})\Delta\theta$ with $\Delta\theta = 2\pi/72$. This grid spacing ensures that in the region, where the major and the minor grids overlapped, grid spacings in the two different grids would be comparable. Away from this region, grid spacings steadily increased from b to $7.5b$. In this study the number of grid points and their distributions were determined by using the minimum values just stated for IL, JL, KL, P, and b.

With the domain size and grid distribution just given, the computed drag coefficient and point of separation compare very well

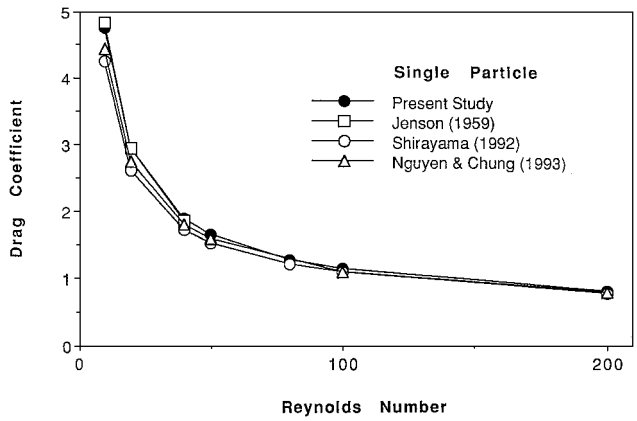

Fig. 5 Drag coefficient C_D as a function of particle Reynolds number *Re* for steady uniform flow past a single particle.

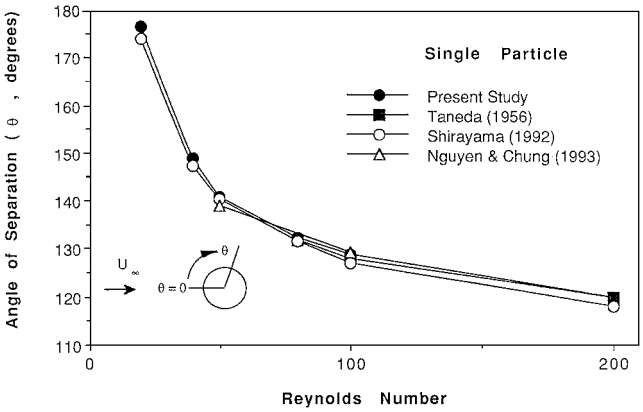

Fig. 6 Angle of separation as a function of particle Reynolds number *Re* for steady uniform flow past a single particle.

with those in the literature. Figures 5 and 6 show that for particle Reynolds number ranging from 10 to 200 the computed results are within 1% of the data published in Refs. 25–28. This close agreement gives some confidence to the modified OVERFLOW code for computing flow past particles. In these figures the symbols represent the Reynolds number at which computations are made and data are available. The lines through the symbols are based on linear interpolation.

Recall that grid spacings in the streamwise direction are constant in the region about the particles but became larger as the distance from the leading or trailing particle increased. Because velocity fluctuations in terms of frequency/wavelength and amplitude imposed at the inflow boundary can change as it is propagated into the domain when grid spacings change in the streamwise direction, it is important to assess the effects of smoothness in grid spacing (i.e., $S = \Delta x_{i+1}/\Delta x_i$) on frequency/wavelength and amplitude. Numerical experiments conducted with the particles removed showed that when $S = 1.2$ the amplitude reduced by less than 10% from inflow to outflow. The frequency/wavelength was found to be within 1%. Finally, the wave form was found to be nearly sinusoidal in the region about the particles because the fluctuations were small (5% of mean flow). In this study S was set equal to 1.2.

Results

Numerical solutions were obtained to investigate the effects of flow past stationary spherical particles with and without fluctuation to understand how wavelength of velocity fluctuation affect drag, surface pressure, and surface shear for three particle problems: single-particle, particles-in-tandem, and particle-array. The results generated for each of these problems are given in Figs. 7–14 and Tables 1–3.

Table 1 Summary of drag,[a] pressure drag, and friction drag coefficients for the single-particle problem at *Re* = 100

λ	$\bar{C}_D$	$\bar{C}_{D,p}$	$\bar{C}_{D,f}$
$2D$	1.17	0.578	0.591
$4D$	1.26	0.649	0.601
$5D$	1.25	0.641	0.601
$7D$	1.22	0.618	0.597
$10D$	1.18	0.591	0.595

[a] $C_D = 1.10$, if there is no fluctuating velocity.

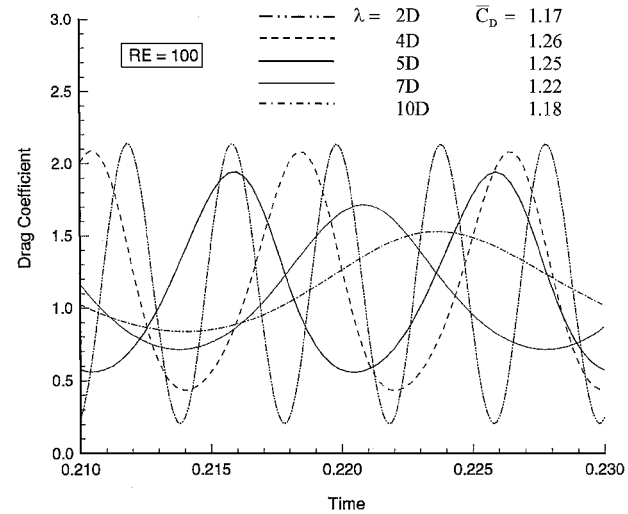

Fig. 7 Drag coefficient C_D as a function of time and $\bar{C}_D$: *Re* = 100, single-particle problem. $\bar{C}_D = C_D = 1.10$ for steady uniform flow.

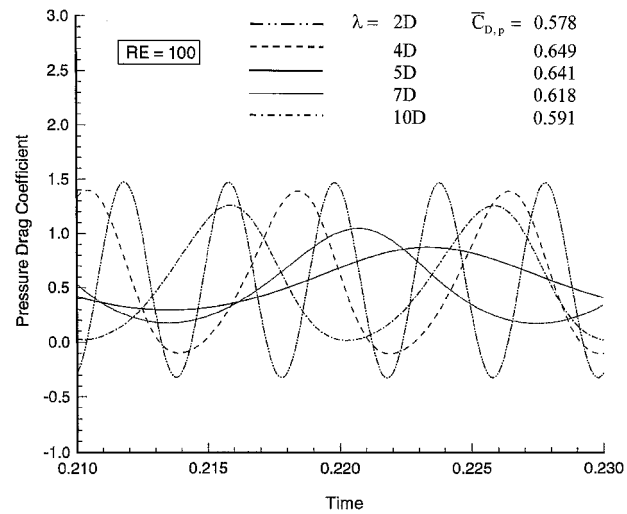

Fig. 8 Pressure drag coefficient $C_{D,p}$ as a function of time and $\bar{C}_{D,p}$: *Re* = 100 and single-particle problem.

Single-Particle Problem

For the single-particle problem the Reynolds number was kept at 100, and the following λ were investigated: $2D$, $4D$, $5D$, $7D$, and $10D$. Results for the single-particle problem are given in Figs. 7–11 and Table 1. Figures 7–9 show C_D, $C_{D,f}$, and $C_{D,p}$ as a function of time. Figures 10 and 11 show C_f and C_p on the particle surface as a function of azimuthal angle along a plane that cuts through the center of the particle, where 0 and 180 deg correspond to forward and rear stagnation points, respectively. Only the time periodic solutions are given.

From Figs. 7–11 and Table 1, several observations can be made. The first observation is that the velocity fluctuation given by Eq. (1)

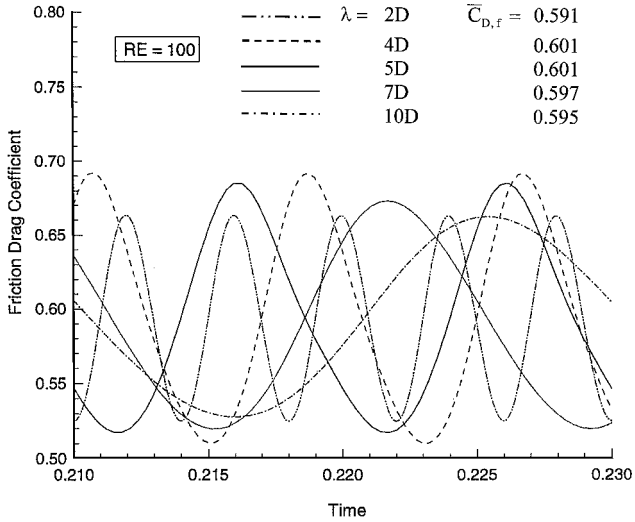

Fig. 9 Friction drag coefficient $C_{D,f}$ as a function of time and $\bar{C}_{D,f}$: $Re = 100$ and single-particle problem.

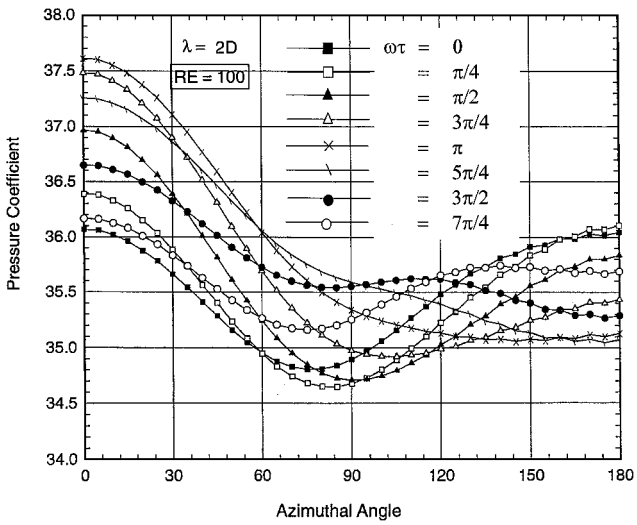

a) $\lambda = 2D$

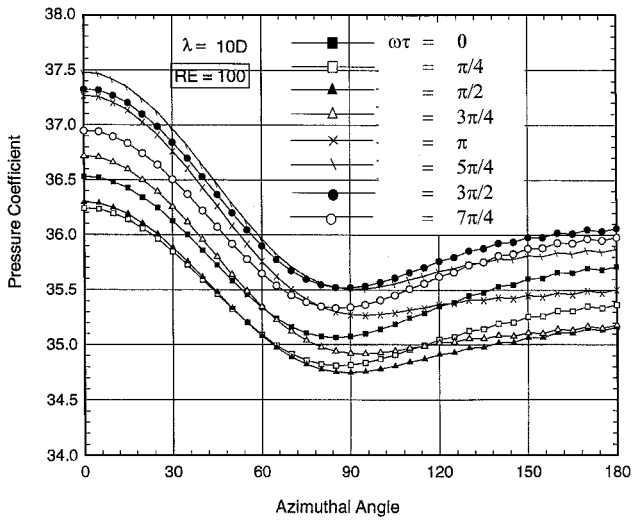

b) $\lambda = 10D$

Fig. 10 Pressure coefficient C_p as a function of azimuthal angle for the single-particle problem.

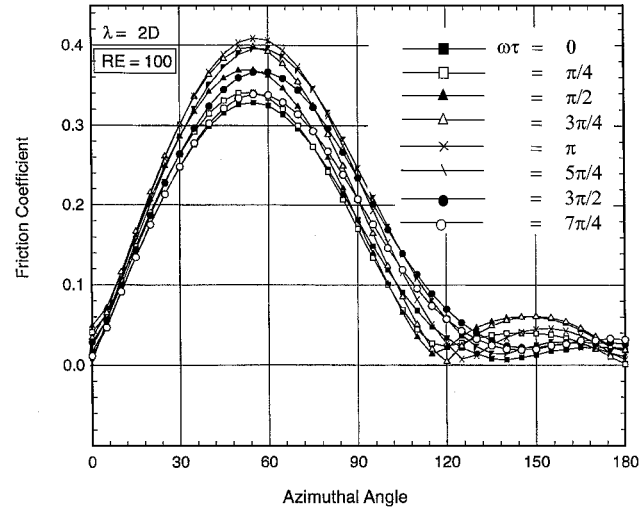

a) $\lambda = 2D$

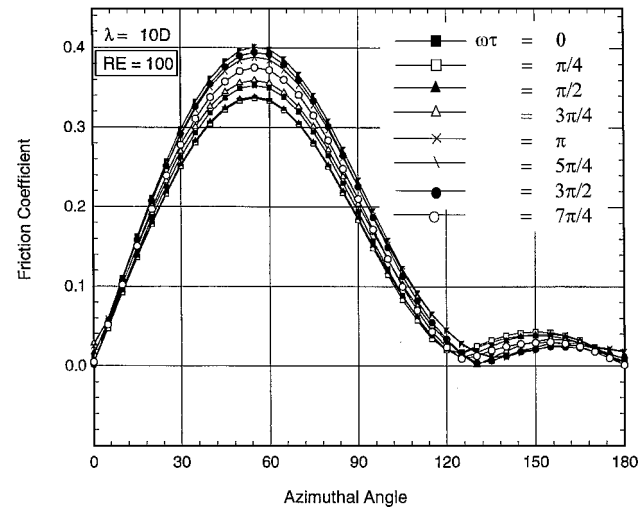

b) $\lambda = 10D$

Fig. 11 Friction coefficient as a function of azimuthal angle at several $\omega\tau$ for the single-particle problem.

causes C_D, $C_{D,f}$, and $C_{D,p}$ to oscillate (Figs. 7–9). This is expected because fluctuating velocity about a particle can induce oscillations in surface pressure and shear stress.

The second observation is that the amplitude of oscillation in C_D and $C_{D,p}$ decreases as λ increases from $2D$ (Figs. 7 and 8). This is also expected because higher λ implies lower energy content in the flow.

The third observation is that the amplitude of oscillation in $C_{D,f}$ has a maximum near $\lambda = 4D$ (Fig. 9). In the legend of Fig. 9, it can be seen that $\bar{C}_{D,f}$ (the average $C_{D,f}$ over its period of oscillation) also has a maximum near $\lambda = 4D$ with $\bar{C}_{D,f}$ dropping faster in value when λ decreases than when λ increases. These results for $C_{D,f}$ and $\bar{C}_{D,f}$ indicate that below a certain λ the flow tends to dissipate the energy more rapidly than does the particle.

The fourth observation is that $\bar{C}_D$ and $\bar{C}_{D,p}$ (average C_D and $C_{D,p}$ over the period of oscillation), given in the legends of Figs. 7–9, also exhibit a maximum around $\lambda = 4D$. This maximum can be attributed in part to the difference between the pressure at the forward and rear stagnation points caused by the oscillating velocity, which is maximum at $\lambda = 4D$.

The fifth observation is that when $\lambda \geq 5D$, $C_{D,p} > 0$ during the entire period. But, when $\lambda = 2$ and $4D$, $C_{D,p}$ can be negative during part of the period. To understand why $C_{D,p}$ can be negative when $(u_0 - u') > 0$, C_p and C_f need to be examined. From Fig. 10a it can be seen that when $\lambda = 2D$, C_p shows almost complete pressure recovery at the rear stagnation point at $\omega\tau = 0$. As $\omega\tau$ increases, the recovery drops then rises in a periodic manner. This higher than

Table 2 Summary of drag coefficient for the particles-in-tandem problem

Which particle?	$\bar{C}_D$ fluctuating ($\lambda = 2D$)	C_D nonfluctuating
1st	1.059	1.065
2nd	0.474	0.528
3rd	0.496	0.585
4th	0.546	0.691

Table 3 Summary of drag coefficient for the 3rd particles in the particle-array problem

α	Re	λ	$\bar{C}_D$	C_D[a]
0.0198	50	$2D$	1.28	1.28
0.0198	100	$2D$	0.77	0.81
0.0198	100	$10D$	0.78	——
0.065	50	$2D$	1.73	1.76
0.065	100	$2D$	1.00	1.05
0.065	100	$10D$	1.01	——
0.098	50	$2D$	2.07	2.10
0.098	100	$2D$	1.22	1.29
0.098	100	$10D$	1.23	——

[a] C_D is drag coefficient with no fluctuating flow (i.e., $\omega = 0$).

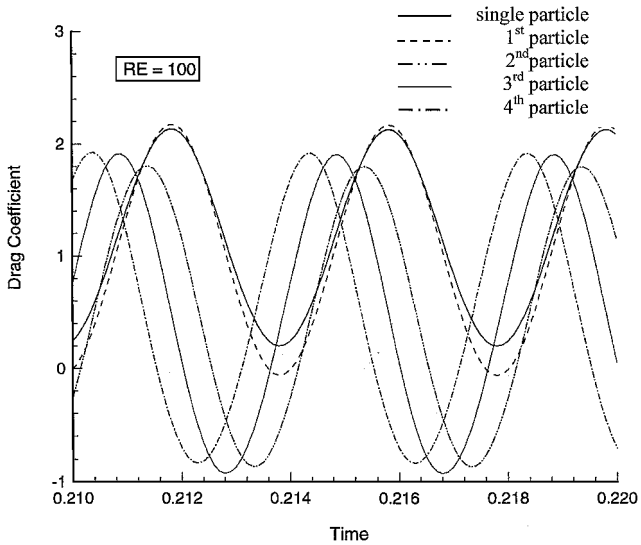

Fig. 12 Drag coefficient C_D as a function of time for single-particle and particles-in-tandem problems at $Re = 100$ and $\lambda = 2D$.

expected pressure recovery implies that the fluctuating velocity is pushing the point of flow separation further downstream. This can be verified by examining C_f because $C_f = 0$ is the point of flow separation. In Fig. 11a, however, the point of separation is given by the minimum in C_f because the point of flow separation may not be captured at a grid point. Figures 10a and 11a for $\lambda = 2D$ should be contrasted with Figs. 10b and 11b for $\lambda = 10D$. Clearly, when $\lambda = 10D$ both the pressure recovery and the point of separation are not significantly affected by the oscillating velocity.

Finally, for the λ investigated, the average C_D for oscillating flow is always higher than the $\bar{C}_D$ for uniform flow (Table 1).

Particles-in-Tandem Problem

For the particles-in-tandem problem the following parameters were investigated: $Re = 50$ and 100 with and without velocity fluctuation. When there is fluctuation, $\lambda = 2D$ and $10D$. Results for the particles-in-tandem problem are given in Figs. 12 and 13 and Table 2. Only the time periodic solutions are presented.

Figures 12 and 13 show that similar to the single-particle problem the oscillating velocity causes oscillations in C_D, and the amplitude of that oscillation decreases as λ increases and as Reynolds number decreases. The differences between the single-particle problem and

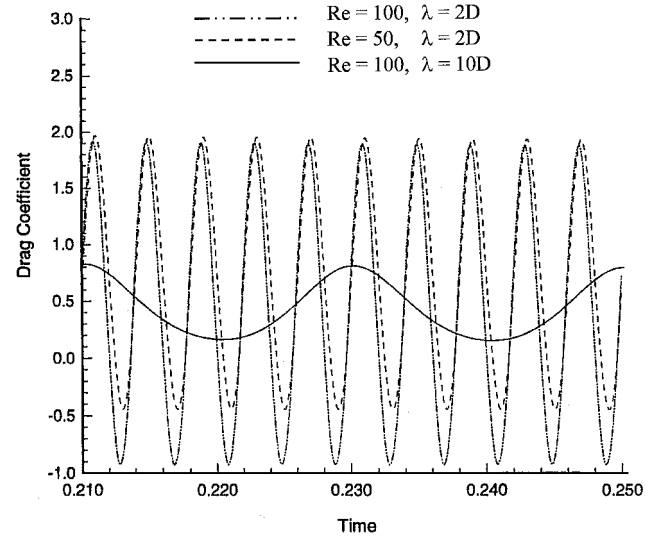

Fig. 13 Drag coefficient C_D of the third particle in the particles-in-tandem problem as a function of time.

the particles-in-tandem problem are as follows. First, $\bar{C}_D$ for fluctuating flow is lower instead of higher than that for uniform flow (Table 2). Second, when $Re = 100$ and $\lambda = 2D$, C_D can be negative during part of the period. For the single-particle problem C_D is positive during the entire period (only $C_{D,p}$ could be negative). These two results indicate that particle/particle interactions affect how a fluctuating velocity affects the point of flow separation and the pressures at the forward and rear stagnation points through changes in the local flow velocity.

Finally, the variations in $\bar{C}_D$ and C_D can be very different from each other (see Fig. 12). For $\bar{C}_D$, the variation is as follows: it drops sharply from the first to the second particle; rises slightly from the second to the third particle; and rises sharply from the third to the last particle. This observed variation in $\bar{C}_D$ from particle to particle is the same whether the flow is fluctuating or not. The high drag coefficient associated with the first or leading particle is because it sees the highest stagnation pressure on the part of the surface facing the oncoming flow (leading surface). The drag coefficient drops sharply on the second particle because the stagnation pressure on its leading surface is considerably lower. The drag coefficient rises on the last or trailing particle because the wake behind that particle can develop fully giving rise to higher pressure drag.

As mentioned, the variation in C_D (the instantaneous drag coefficient) can be quite different from that of $\bar{C}_D$, when there is a fluctuating flow. For C_D, the variation depends on time. For example, at nondimensional time = 0.212 (Fig. 12) C_D is a monotonic function of the particle with C_D being the highest for the first particle and the lowest for the last particle. At nondimensional time = 0.214, the fourth or last particle has the highest C_D, and this is followed by the third particle, the first particle, and finally the second particle. This observed difference between $\bar{C}_D$ and C_D results because different particles along the flow direction see different parts of the fluctuating flowfield.

The variation in drag coefficient and hence drag from particle to particle has important consequences on whether the particles collide or separate. Because the particles in this study do not move, only the initial tendency to collide or separate can be inferred.

Particle-Array Problem

For the particle-array problem, the following parameters were investigated: $Re = 50$ and 100; $\lambda = 2D$ and $10D$; $\alpha = 0.0198, 0.065$, and 0.098. Results for the particle-array problem are given in Fig. 14 and Table 3.

Figure 14 shows C_D as a function of time. From this figure, it can be seen that similar to the single-particle and particles-in-tandem problems, fluctuations in the velocity induce oscillations in C_D. The amplitude of this oscillation in C_D was found to

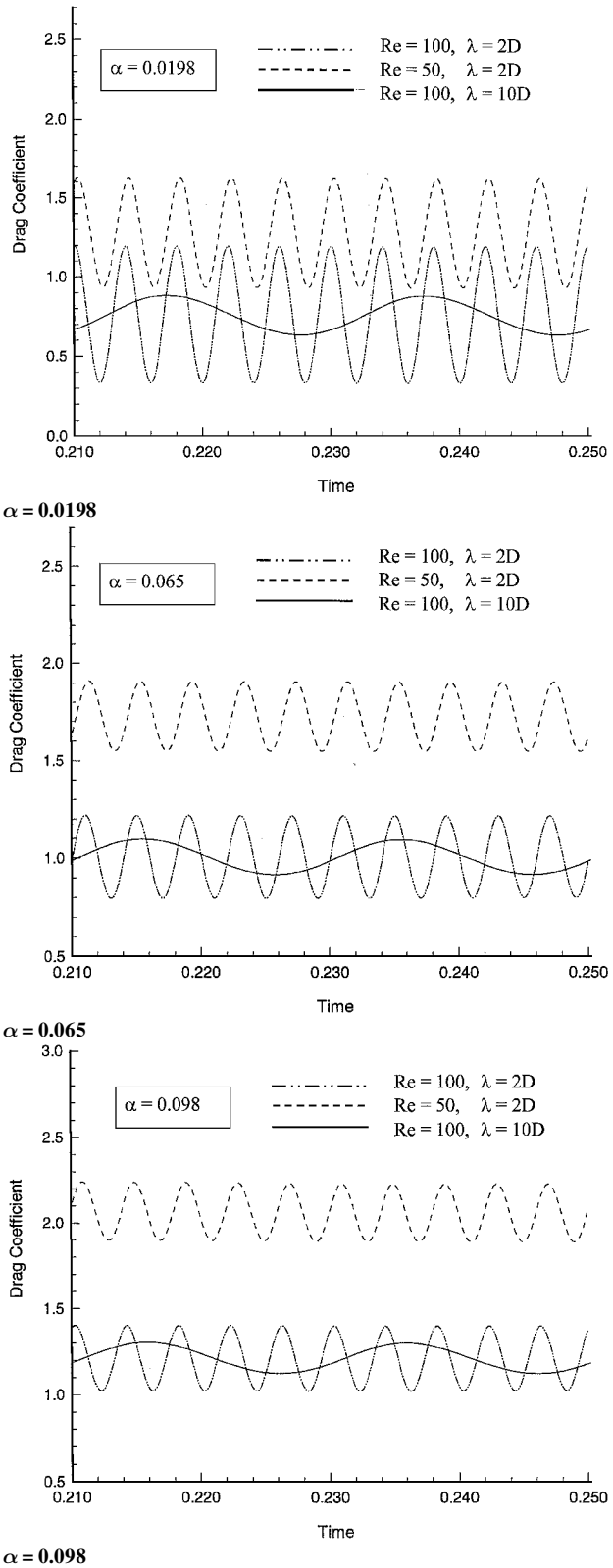

Fig. 14 Drag coefficient C_D of the third particle in the particle-array problem as a function of time.

decrease as λ increases, as the Reynolds number decreases, and as α increases. $\bar{C}_D$ was found to increase as λ, Reynolds number, and α increase (Table 3). However, the dependence on λ is very weak; i.e., the changes in $\bar{C}_D$ are small as λ is varied. In fact, at $Re = 50$, $\bar{C}_D$ for fluctuating and nonfluctuating flows are about the same. This is markedly different from that observed for the particles-in-tandem problem. This difference is caused by the difference in particle/particle interactions from different particle arrangements.

Not shown is that particles can create considerable disturbances on the flow. Deviation from the mean freestream velocity, $k_p = [(u-u_0)^2 + v^2 + w^2]^{1/2}$, can be interpreted as the turbulent kinetic energy produced by the particles (i.e., turbulence modulation). Results obtained show that k_p can be as high as 5% for the volume fractions and particle Reynolds numbers investigated. For a given Reynolds number and different α the length scales of the disturbed flow were found to be proportional to the particle diameter and the spacing between particles. The deviation from the freestream mean x-component velocity, $u - u_0$, is useful in revealing how particles disturb the flow.

Conclusions

Velocity fluctuations can affect significantly C_D, $C_{D,p}$, $C_{D,f}$, C_p, and C_f by shifting the point of flow separation and by altering the pressure at the forward and rear stagnation points. When there are neighboring particles, fluctuating flow can produce negative C_D because of particle/particle interactions. Finally, particles can produce considerable disturbances to the flow (turbulence modulation) with the length scales proportional to the particle diameter and spacing between particles.

References

[1]Mulholland, J. A., Srivastava, R. K., and Wendt, J. O. L., "Influence of Droplet Spacing on Drag Coefficient in Nonevaporating, Monodisperse Streams," *AIAA Journal*, Vol. 26, No. 10, 1988, pp. 1231–1237.

[2]Poo, J. Y., and Ashgriz, N., "Variation of Drag Coefficients in an Interacting Drop Stream," *Experiments in Fluids*, Vol. 11, No. 1, 1991, pp. 1–8.

[3]Kladas, D. D., and Georgiou, D. P., "A Relative Examination of C–Re Relationships Used in Particle Trajectory Calculation," *Journal of Fluids Engineering*, Vol. 115, No. 1, 1983, pp. 162–165.

[4]Roco, M. C. (ed.), *Particulate Two-Phase Flow*, Butterworth-Heinemann, Boston, 1993.

[5]Kim, S., and Russel, W. B., "Modelling of Porous Media by Renormalization of the Stokes Equations," *Journal of Fluid Mechanics*, Vol. 154, 1985, pp. 269–286.

[6]Kim, S., and Karrila, S. J., *Microhydrodynamics: Principles and Selected Applications*, Butterworth-Heinemann, Boston, 1991.

[7]Kim, H. S., and Prosperetti, A., "Numerical Simulation of the Motion of Rigid Spheres in Potential Flow," *SIAM Journal of Applied Mathematics*, Vol. 52, No. 6, 1992, pp. 1533–1562.

[8]Ramachandran, R. S., Wang, T.-Y., Kleinstreuer, C., and Chiang, H., "Laminar Flow past Three Closely Spaced Monodispersed Spheres or Nonevaporating Drops," *AIAA Journal*, Vol. 29, No. 1, 1991, pp. 43–51.

[9]Nirschl, H., Dwyer, H. A., and Denk, V., "A Chimera Grid Scheme for the Calculation of Particle Flows," AIAA Paper 91-0519, 1991.

[10]Deng, Z. T., and Jeng, S.-M., "Numerical Simulation of Droplet Deformation in Convective Flows," *AIAA Journal*, Vol. 30, No. 5, 1992, pp. 1290–1297.

[11]Sirignano, W. A., "Fluid Dynamics of Sprays—1992 Freeman Scholar Lecture," *Journal of Fluids Engineering*, Vol. 115, No. 3, 1993, pp. 345–378.

[12]Chiang, C. H., and Sirignano, W. A., "Axisymmetric Calculations of the Three-Droplet Interactions," *Atomization and Sprays*, Vol. 3, No. 1, 1993, pp. 91–107.

[13]Kim, I., Elghobashi, S. E., and Sirignano, W. A., "Three-Dimensional Flow over Two Spheres Placed Side by Side," *Journal of Fluid Mechanics*, Vol. 246, 1993, pp. 465–488.

[14]Feng, J., Hu, H. H., and Joseph, D. D., "Direct Simulation of Initial Value Problems for the Motion of Solid Bodies in a Newtonian Fluid. Part 2: Couette and Poiseuille Flows," *Journal of Fluid Mechanics*, Vol. 277, 1994, pp. 271–301.

[15]Dasgupta, A., Shih, T. I-P., Kundu, K. P., and Deur, J. M., "Numerical Simulation of Flow past an Array of Moving Spherical Particles," AIAA Paper 94-3283, June 1994.

[16]Lin, Y.-L., Shih, T. I-P., and Jhon, M. S., "Computations of Drag and Lift on a Rotating Sphere in a Constant Shear Flow," AIAA Paper 96-0082, Jan. 1996.

[17]Johnson, A. A., and Tezduyar, T. E., "3D Simulation of Fluid-Particle Interactions with the Number of Particles Reaching 100," *Computer Methods in Applied Mechanics and Engineering*, Vol. 145, 1997, pp. 301–321.

[18]Shih, T. I-P., "Modeling Multiphase Flows Through Direct Numerical Simulation," American Society of Mechanical Engineers, FEDSM 98-5039, June 1998.

[19]Duvvur, A., Chiang, C. H., and Sirignano, W. A., "Oscillatory Fuel Droplet Vaporization: Driving Mechanism for Combustion Instability," *Journal of Propulsion and Power*, Vol. 12, No. 2, 1996, pp. 358–365.

[20]Anderson, D. A., Tannehill, J. C., and Pletcher, R. H., *Computational Fluid Mechanics and Heat Transfer*, Hemisphere, Washington, DC, 1984.
[21]Bunning, P. G., and Chan, W. M., "OVERFLOW/F3D User's Manual," NASA Ames Research Center, Moffett Field, CA, March 1991.
[22]Pulliam, W. R., and Chaussee, D. S., "A Diagonal Form of an Implicit Approximate-Factorization Algorithm," *Journal of Computational Physics*, Vol. 39, No. 2, 1981, pp. 347–363.
[23]Benek, J. A., Buning, P. G., and Steger, J. L., "A 3-D Chimera Grid Embedding Technique," AIAA Paper 85-1523, July 1985.
[24]Benek, J. A., Donegan, T. L., and Suh, N. E., "Extended Chimera Grid Embedding Scheme with Application to Viscous Flows," AIAA 87-1126, June 1987.
[25]Taneda, S., "Experimental Investigation of the Wakw Behind a Sphere at Low Reynolds Numbers," *Journal of the Physical Society of Japan*, Vol. 11, No. 10, 1956, pp. 1104–1108.
[26]Jenson, V. G., "Viscous Flow Around a Sphere at Low Reynolds Numbers," *Proceedings of the Royal Society of London*, Vol. 249A, 1959, pp. 346–366.
[27]Shirayama, S., "Flow past a Sphere: Topological Transitions of the Vorticity Field," *AIAA Journal*, Vol. 30, No. 2, 1992, pp. 349–358.
[28]Nguyen, H. D., and Chung, J. N., "A Chebyshev-Legendre Spectral Method for the Transient Solution of Flow past a Solid Sphere," *Journal of Computational Physics*, Vol. 104, No. 2, 1993, pp. 303–312.